Journal of Magnetic Resonance 255 (2015) 100–105

Contents lists available at ScienceDirect

Journal of Magnetic Resonance

journal homepage: www.elsevier.com/locate/jmr

An ultra-low cost NMR device with arbitrary pulse programming

Hsueh-Ying Chen [a], Yaewon Kim [a], Pulak Nath [b], Christian Hilty [a,*]

[a] Chemistry Department, Texas A&M University, College Station, TX 77845-3255, USA
[b] Los Alamos National Laboratory, Los Alamos, NM 87545, USA

ARTICLE INFO

Article history:
Received 26 November 2014
Revised 14 February 2015
Available online 10 March 2015

Keywords:
NMR hardware
Relaxometry
Portable NMR

ABSTRACT

Ultra-low cost, general purpose electronics boards featuring microprocessors or field programmable gate arrays (FPGA) are reaching capabilities sufficient for direct implementation of NMR spectrometers. We demonstrate a spectrometer based on such a board, implemented with a minimal need for the addition of custom electronics and external components. This feature allows such a spectrometer to be readily implemented using typical knowledge present in an NMR laboratory. With FPGA technology, digital tasks are performed with precise timing, without the limitation of predetermined hardware function. In this case, the FPGA is used for programming of arbitrarily timed pulse sequence events, and to digitally generate required frequencies. Data acquired from a 0.53 T permanent magnet serves as a demonstration of the flexibility of pulse programming for diverse experiments. Pulse sequences applied include a spin–lattice relaxation measurement using a pulse train with small-flip angle pulses, and a Carr–Purcell–Meiboom–Gill experiment with phase cycle. Mixing of NMR signals with a digitally generated, 4-step phase-cycled reference frequency is further implemented to achieve sequential quadrature detection. The flexibility in hardware implementation permits tailoring this type of spectrometer for applications such as relaxometry, polarimetry, diffusometry or NMR based magnetometry.

1. Introduction

Low cost nuclear magnetic resonance (NMR) devices are experiencing considerable publicity, both in an industrial and academic setting. A number of commercial systems are available, and in addition, published designs are readily found in the literature. These devices cater to opposing trends, for emerging routine applications where simplicity in operation is a must, as well as for ancillary characterizations in NMR or MRI experiments that are growing more and more complex. Examples for the first category include industrial quality control, for example the determination of fat or water content using spin relaxation measurements [1–5]. They further include the characterization of objects containing large surfaces [6], the determination of oil or water content in rock surrounding a borehole [7], or the detection of cells and biomarkers for biomedical applications [8]. Finally, a multitude of educational applications benefit from low-cost NMR devices, for teaching aspects of instrumentation, NMR theory, or molecular structure determination [9–12]. In many cases, the achieved ease of use betrays an increasing sophistication of these devices. In the second category, low-cost NMR devices are supportive in the characterization of more elaborate magnetic resonance experiments. An example is the use of a dedicated spectrometer accessory for the determination of magnetic field profiles, which can be used to improve the quality of high resolution magnetic resonance images [13,14]. Ancillary NMR spectrometers are also used in the growing field of hyperpolarized NMR, for monitoring the spin polarization that is achieved. Optical pumping experiments often include NMR devices at the pumping cell for polarimetry [15,16]. In dissolution dynamic nuclear polarization, monitoring of NMR signals is desirable both during polarization in the solid state, as well as after dissolution in the liquid state [17].

A range of standalone NMR devices have been developed in view of these varied applications. Many of the recent implementations make use of a microcontroller for flexibility in programming [18,19], or include parallel processing capabilities of field programmable gate arrays (FPGA) in designs similar to those of software based radios [20–24]. Such devices have been developed to the level, where they can serve as budget NMR consoles for high-field NMR applications at frequencies of hundreds of megahertz [25].

An increasing number of non-specialized, but pre-fabricated hardware boards that feature microprocessors or FPGA chips are becoming available in the market at ultra-low cost. The use of such boards for NMR applications is interesting, because they can allow

* Corresponding author.
E-mail address: chilty@tamu.edu (C. Hilty).

http://dx.doi.org/10.1016/j.jmr.2015.02.011
1090-7807/

the creation of functional NMR devices without the need for large designs of custom electronics. A spectrometer developed based on an arduino board has recently been introduced to acquire signals from earth field NMR [26]. At higher frequencies, in the range of tens to hundreds of megahertz, FPGAs are more suitable than microprocessors, because of their support for parallel processing and increased control of accurate timing. Here, we demonstrate the acquisition of relaxometry data using a spectrometer constructed from a single commercial FPGA board, which already contains required components such as digitizer, clock, memory, programming and communications interface, and for use in NMR only requires the addition of analog front-end circuits. The console is optimized for maximum flexibility by implementing most functions within the FPGA chip. With this simplicity and flexibility, a rapid and application oriented implementation of the NMR spectrometer is possible.

2. Materials and methods

The console hardware is based on an Altera Cyclone IV field programmable gate array (FPGA) with the DE0-nano evaluation board ($75 \times 50 \times 20$ mm, Terasic, Hsinchu City, Taiwan), which contains all digital signal pathways. In the FPGA, custom logic for pulse program generation and data storage is implemented (Fig. 1). Also within the FPGA, this logic is supported by an array of standard blocks performing functions such as frequency generation, communication or memory access.

The NMR pulse program is executed using the custom logic blocks. Before the NMR scan, the program is loaded into memory as a list of system states each associated with a time. Such system states include no output during a waiting time, activation of a transmit/receive switch, application of a pulse with a phase selected from one of four options ($+x$, $+y$, $-x$, $-y$), or digitization of data. In the memory, these system states are simply represented

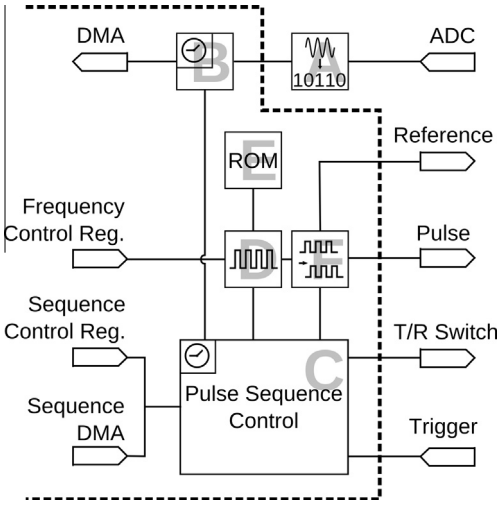

Fig. 1. Components of the FPGA design. The components inside of the dashed line are implemented in the FPGA. Signals are acquired using an analog-to-digital converter (A) on the DE0 board, captured in the FPGA in a block clocked at the sampling frequency (B) and streamed to memory. The pulse sequence events are streamed from the memory to a pulse sequence controller (C) under control of a pulse sequence clock. The signal frequency is generated in a phase locked loop (D), which is configured with predetermined parameters stored in ROM (E) and phase shifted (F) under pulse sequence control. The terminals drawn on the left side interface to registers and DMA controllers realized as standard blocks within the FPGA design, and are under the control of a CPU (not shown). The pulse sequence and frequency control registers are used to set parameters that do not change during pulse sequence execution. The terminals to the right interface to those shown in Fig. 2.

as a 32-bit time stamp associated with a 32-bit control word. Before the start of the experiment, a number of additional, asynchronous settings can be configured. This configuration includes setting ancillary parameters, such as whether an external trigger is used ('sequence control register'), and selecting reference and pulse frequency ('frequency control register'). For frequency selection, a phase locked loop (PLL) is configured with predetermined parameters stored in a table within the memory, which allows derivation of a desired excitation frequency ('transmitter clock').

After the start of the experiment, the system states contained in the pulse program are autonomously played back with accurate timing within the FPGA. Playback of the pulse sequence is achieved using a direct memory access (DMA) controller programmed in the FPGA. In this design, even the time resolution of the device is reconfigurable, by changing the speed of the clock used for timing of the pulse sequence events. In the present experiments, a 'sequence clock' of 10 MHz or 20 MHz is derived from a PLL implemented in the FPGA, that is driven by a physical on-board clock operating at 50 MHz. Due to the capability of running a clock at high frequency, the digital waveform for the NMR excitation pulses (20–30 MHz in the present case) can be directly generated, without the need for up-mixing with frequencies synthesized externally.

Data is acquired from the on-board digitizer and is placed into memory using a DMA controller. The digitizer on the board employs a sampling rate of 200 kHz, which is derived from the 'sequence clock'. This sampling rate is likely sufficient for most applications. It could be increased by interfacing an external digitizer to available pins on the FPGA board. Since all of the clock signals are derived from the same source, phase stability is ensured, enabling reproducible signal averaging.

The settings that are configured prior to execution of the pulse program, as well as loading the pulse program directly into the memory, are achieved using a soft-processor directly embedded in the FPGA. The same processor is used to read the data from the memory, sending it to a host computer via a universal serial bus (USB) interface. Such a soft-processor, capable of (asynchronously) executing a high-level program, is convenient for this purpose. It is, however, not strictly required – the same functions could be performed equally well by a simpler custom logic programmed into the FPGA.

An analog circuit board containing a set of filters, level shifters and amplifiers is still required, however can rapidly be designed with knowledge present in a typical NMR laboratory (Fig. 2). This board in our current implementation contains signal pathways for two transmitter channels and 8 receiver channels. The radio-frequency (RF) signal path is typical for a spectrometer with heterodyne detection. However, a simplification arises from the ability to generate high-frequency digital signals with a defined phase directly within the FPGA using a PLL. Hence, the RF pulse is directly produced as a digital signal at the intended frequency (here, 22 MHz), and is converted into a sine wave by passing through an amplifier (MAX4384EUD+; Maxim Integrated, CA) and a bandpass filter (PBP-21.4+; Mini-Circuits, NY). The reference signal for mixing is generated in the same way. The reference frequency can be set independently if necessary.

In the transmitter pathway, a small radio-frequency amplifier is attached externally (ZHL-3A+; Mini-Circuits) and connected through an active transmit-receive switch (ZX80-DR230+, Mini-Circuit) to the probe. The output power is 30 dBm (1 W in a 50 Ω system). Although FPGA board and console do not include digital-to-analog converters (DAC) for control of pulse amplitudes, the amplitude of all of the pulses in an experiment can be digitally set by changing the duty cycle of the digital signal that is used to generate the pulses. The final pulse amplitude is the result of passing the duty-cycle adjusted digital waveform through the analog filter on the circuit board. In the receiver pathway, external

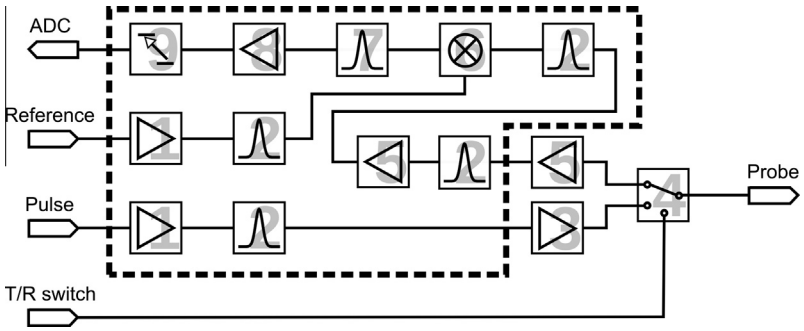

Fig. 2. Components of spectrometer mounted outside of the commercial FPGA board. The dashed border encloses a custom electronics board with surface mount components, while the components outside are discrete. Shown are CMOS signal amplifier (1), radio-frequency bandpass filter (2), pulse amplifier (3), active transmit/receive switch (4), signal pre-amplifier (5), mixer (6), low-frequency bandpass filter (7), low-frequency signal amplifier (8), and CMOS signal level shifter (9). The terminals to the left interface to those shown in Fig. 1.

pre-amplifiers (ZFL-500LN+; Mini-Circuits) and filters (PBP-21.4+; Mini-Circuits) condition the signal before mixing (ADE-1L+; Mini-Circuits, NY). Including external and on-board pre-amplifiers, a total gain up to 118 dB is obtained.

After down-mixing the signal frequency, an active band-pass filter at the low frequency (MAX274A; Maxim Integrated) ensures that noise is not folded into the detected frequency range. Various types of active filters can be set by an external resistor network (as indicated in the supporting material). Here, the Chebyshev filter is chosen due to the feature of sharp cut-off edge of transmission. This filter is followed by a final stage of amplification, shifting to CMOS signal level (0–3.3 V), and digitization. The analog circuit board was assembled making use of surface mount technology. As shown in Fig. 3a, the FPGA board is integrated into the main circuit board. On-board preamplifiers for each detection channel are indicated by red[1] rectangles. Up to eight channels can be implemented on the circuit board. It is possible to use these channels for simultaneous measurements that require multiple receivers at the same frequency, or to implement different RF filters, such that channels for different frequencies are available. The electronics for the low frequency signals after mixing are placed in the center region of the board, close to the inputs of the ADC. Despite including multiple channels for data acquisition, the entire NMR console remained compact, at a dimension of $20 \times 18 \times 10$ cm.

Data shown in Figs. 4–6 were acquired using a small permanent magnet of the 'shim-a-ring' design [27]. This magnet geometry consists of a cylindrical rare earth magnet magnetized perpendicular to the bore. The magnet is seated in a ring made of soft iron, which results in a homogeneous field throughout the bore. The assembly of the two parts takes place automatically due to their mutual attraction (see the video included in the supporting material). Compared to common permanent magnets (e.g. Halbach cylinders [28]), the 'shim-a-ring' design reduces the need for manually aligning multiple magnets, and thereby significantly reduces the cost of a suitable magnet for NMR application. The dimensions of this magnet were 76 mm (outer diameter of iron ring), 32 mm (outer diameter of rare earth magnet), 10 mm (diameter of bore) and 50.8 mm (thickness of magnet). The magnetic field within the bore was 0.53 T, resulting in a ^{1}H NMR frequency of 22.7 MHz. This magnet was grounded to the spectrometer in all experiments, which significantly reduced noise.

The NMR coil used for acquiring the data contained 8 turns of copper wire, length 0.5 mm, on a fused silica capillary with 360 μm outer diameter and 250 μm inner diameter. The active sample volume of the coil was 25 nL. The microcoil was tuned and matched using variable capacitors that were placed as close as possible to the probe (Fig. 3b). In an ideal 'shim-a-ring' magnet, the magnetic field is nearly constant within the bore. Practically, the region of highest magnetic field homogeneity was found using a translational stage or a microcoil holder composed of two interlocking, rotatable cylinders, one of which was shifted off-axis to allow the coil to reach any position within the bore of the magnet.

Limited to the conversion rate of the ADC (f_{ADC} = 200 ksps, ADC128S022, National Semiconductor) built into the DE0-nano board, an analog mixing method is used for down-conversion of

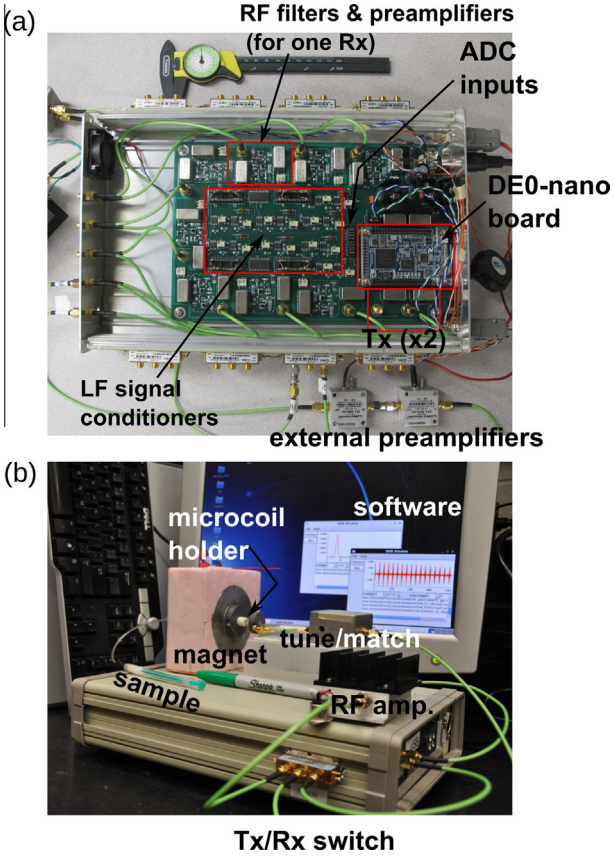

Fig. 3. (a) Interior view of NMR console, showing the DE0-nano FPGA board and the RF components. Components include external pre-amplifiers and electronics for functions such as down-mixing, filtering and amplification. The DE0 board, containing core elements such as FGPA, ADC and oscillator, is connected on top of the circuit board. (b) An overview of the portable NMR apparatus with a RF power amplifier, a magnet and a tune/match accessory on the top of the console. Here, we only have one Tx/Rx switch attached at the side of the case.

[1] For interpretation of color in Fig. 3, the reader is referred to the web version of this article.

the received signal. Acquisition at this frequency makes digital demodulation impractical. It would be possible to use an external ADC to sample at a higher frequency, in which case digital quadrature detection could be performed inside the FPGA. However, quadrature detection is also possible using an alternative method, which was proposed by Bodenhausen et al. [29]. Using a single set of receiver and mixer, the signal at f_{NMR} is mixed with f_{REF} that is phase shifted with $\pi/2$ in each successive acquired data point, resulting in a 4-step cycle. The obtained time domain data array (f_n, $n = 1, 2, \ldots N$) is then rearranged to a complex valued free induction decay (FID) as expressed in Eq. (1), and Fourier transformed into a phase sensitive spectrum. In the process, the NMR frequency offset is modulated with $\frac{1}{4}f_{ADC}$ (f_{ADC} is the digitization rate). Thus, a corresponding center frequency, here 50 kHz, of the pass-band of the low frequency filter (element #7 in Fig. 2) is necessary.

$$\begin{aligned} &\text{Real part}: (-1)^{k-1}\cdot f_{2k-1} \\ &\text{Imaginary part}: (-1)^{k-1}\cdot f_{2k} \\ &k = 1,2,3,\ldots\frac{N}{2} \end{aligned} \tag{1}$$

Quadrature and signal-to-noise performance was compared using an Avance III NMR console and 9.4 T superconducting magnet (Bruker Biospin, Billerica, MA). For this purpose, ^{14}N spectra of an NH_4Cl solution in a broadband observe (BBO) probe (Bruker) were measured using both consoles.

In order to facilitate uploading the pulse program to the DE0 board, as well as downloading the data from memory, a graphical user interface was programmed in a C++ language using GTK+ [30] (Fig. 3b). This interface allows displaying FIDs from an array of experiments as well as simple Fourier transformation and peak integration. For advanced data processing, the FID data was exported from this interface to be processed using MATLAB software (MathWorks, Natick, MA).

3. Results and discussion

To demonstrate the performance of the FPGA-based NMR console, a set of NMR measurements was carried out, including spin-echo and spin–lattice relaxation experiments. These measurements were carried out using a 25 nL microcoil in a small permanent magnet (see Section 2). A sample of paramagnetically doped H_2O was used for the experiments in order to increase repetition rate of the experiment, and at the same time to evaluate the performance of fast averaging. A spin-echo pulse sequence is shown in Fig. 4a. In this experiment, digitization of the NMR signal is enabled both after the $\pi/2$ and π pulses, which in the pulse sequence is achieved simply by switching the corresponding control bit. A dedicated experiment was used for scanning the reference frequency generated in the FPGA for heterodyne detection, to ensure that the down-mixed signal from spin precession in the permanent magnet was located inside of the passband of the final filter stage in the spectrometer. Subsequently, the length for the excitation pulse was calibrated by incrementing its duration. With the determined settings, a clean ^1H signal following the initial excitation and refocusing pulses is observed, shown in Fig. 4b after averaging of 512 scans. Only a small discontinuity appears in the acquired signal, which corresponds to the time required for the π pulse and the latency of switching between transmitter and receiver paths. Typically, this time is set to 20–40 μs, which is sufficient for probe recovery after RF excitation.

After re-enabling the receiver, an initial spike can further be observed in the signal at around 1.3 ms. To discover the source of this artifact, a control experiment, in which the sample and RF pulses are removed, was performed (Fig. 4c). This control experiment suggests that the observed artifact arises from the active

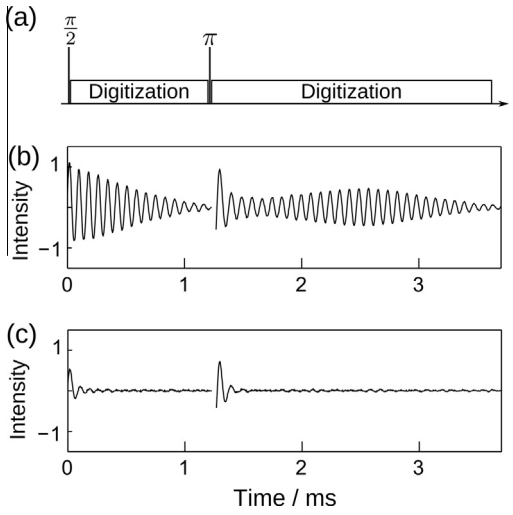

Fig. 4. (a) Spin-echo pulse sequence. (b) NMR signal of water doped with 5% $CuSO_4$ acquired using the sequence in (a). The digitization is enabled after both of the RF pulses with flip angle of $\pi/2$ and π. (c) Background obtained after removing the sample and without applying pulses.

switching between transmitter and receiver (component #4 in Fig. 2). The life time of the ringing signal is governed by the time constant of the active low-pass filter (component #7 in Fig. 2) integrated in the last amplification stage prior to digitizing the signal. This could be reduced by increasing the bandwidth of the receiver, which would however require the use of a digitizer with a faster clock rate.

The experiment shown in Fig. 4 also demonstrates that the NMR console, despite its compactness, still provides sufficient control of timing, duration and frequency of the excitation pulse as well as the reference frequency to be used in the heterodyne detection in the MHz range. Various applications can therefore be explored. Spin relaxation measurements in the low field, for example, have been used extensively in various areas including the food, petroleum and pharmaceutical industries. Due to the abundance of these applications, we have investigated the feasibility of relaxation measurements using this spectrometer. Instead of the conventional inversion-recovery experiment for spin–lattice relaxation measurement, an alternative T_1 measurement using a series of RF excitations with small-flip angle was implemented, which had originally been described by Kaptein et al. [31]. This pulse sequence allows for a rapid analysis of spin relaxation, without the need for incrementing a recovery time delay as would be the case in the inversion-recovery experiment. FIDs are acquired after each of k successive excitations with a recycle delay t_r. As shown in Fig. 5a, the ^1H signals of an aqueous solution containing 0.3% $CuSO_4$ are gradually decaying until reaching a steady-state, where the signal loss due to RF excitation and signal build-up from relaxation recovery compensate. The signal amplitude at this steady-state equilibrium is dependent on the ratio between the spin–lattice relaxation time T_1 and the recycle time t_r. Quantitatively, the T_1 time constant can be obtained by fitting the integrated signals (S_k) to the equation

$$S_k = (\beta c - \beta)\frac{1-(\beta c)^{k-1}}{1-\beta c} + 1 \tag{2}$$

where $\beta = e^{-t_r/T_1}$ and $c = \cos(\alpha)$. In this equation, α is the flip angle of the excitation pulse. Fig. 5b summarizes the obtained T_1 time constants with the standard deviations from three replicates at each recycle delay of 30, 50 and 100 ms. The results show an average measurement error of about 5%, indicating a good stability of the

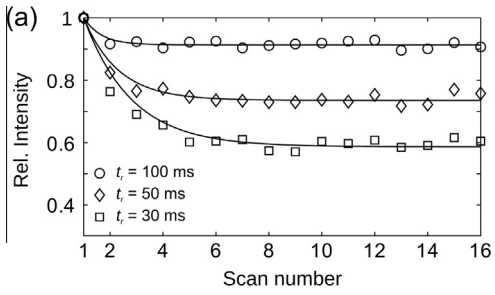

(b)

Recyle delay (t_r, ms)	T_1 relaxation time constant (ms) @ 22.7 MHz
30	104.6 ± 0.85
50	104.5 ± 4.8
100	91.8 ± 6.3

Fig. 5. (a) Measurements of spin–lattice relaxation time (T_1) of 0.3% $CuSO_4$ solution using a series of RF pulses with small-flip angle (45°) with three different recycle delays (t_r). Here, 64 acquisitions are averaged at each recycle delay. (b) Average T_1 relaxation time constants derived from the data in (a) are summarized in the table with the experimental error from three repeated measurements.

signals acquired in the NMR spectrometer. It can be seen that with the longest recycle delay, t_r = 100 ms, the variations in the obtained T_1 are largest. In this measurement, the magnetization recovers almost completely after each RF excitation. Therefore, the difference between the initial amplitude and the amplitude at the steady-state is smallest. Under these conditions, it is reasonable to expect that the accuracy in the T_1 measurement will be affected most strongly by random fluctuations. Consequently, in this experiment, a suitable choice of the recycle delay and small-flip angle is required for an accurate T_1 measurement.

As an additional pulse sequence of interest, we have implemented the Carr–Purcell–Meiboom–Gill (CPMG) experiment, to acquire a train of spin echoes [32]. The CPMG pulse sequence which starts with an initial $\pi/2$ pulse, followed by a series of π pulses, $(\frac{\pi}{2})^y - \tau - (\pi)^x - 2\tau - (\pi)^x - 2\tau \ldots$, is modified from the spin-echo pulse sequence shown in Fig. 4a. It is obtained by repeating the refocusing block $(\tau - (\pi)^x - \tau)$ and enabling the digitization during the echo time (τ). Practically, these repetitive building blocks in the sequence are easily concatenated into a list of events for the pulse programming logic (see Section 2). Fig. 6a displays an echo train, obtained from doped water, which was acquired using eight refocusing blocks and averaged for 32 scans. Again, a clean signal is observed, containing the FID after the initial $\pi/2$ pulse, followed by well resolved echos at 2.5 ms, 5 ms, etc. Still, the aforementioned artifact from the transmit/receive switch is noticeable after each refocusing pulse. This "glitch" might not be problematic when the signal is strong. Nevertheless, with the capability of implementing phase cycles in the pulse program, it is possible to remove these unwanted signals (Fig. 6b).

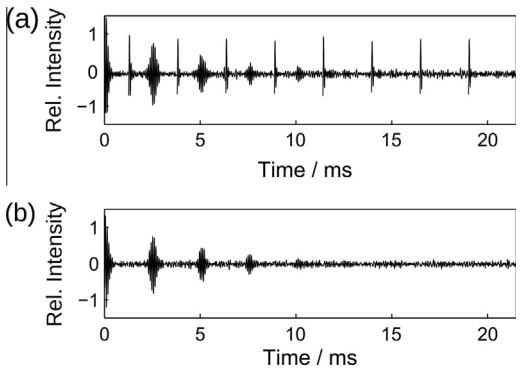

Fig. 6. An echo train obtained from a CPMG pulse sequence without (a) and with (b) the phase cycling from a solution of water doped with $CuSO_4$.

Frequency discrimination was not required, and therefore not implemented in the relaxation measurements described above. In order to demonstrate a data acquisition mode with quadrature detection, as would be desirable for other spectroscopy applications, spectra containing the ^{14}N signal from saturated ammonium chloride (NH_4Cl) in a ~9.4 T superconducting magnet were acquired. This nucleus and field strength were chosen, because the resulting NMR frequency near 30 MHz is close to the 20 MHz proton frequency of the permanent magnet, and at the same time the data can be compared to that of a commercial spectrometer. Quadrature detection was implemented using a single ADC channel with cycling of four phases of the reference signal (see Section 2). Fig. 7a displays the resulting four components of the rearranged FID. This data, acquired as an average of 32 identical scans to improve visibility of the oscillations of the signal in the time domain, shows that the four components of the rearranged FID experience the expected phase shift of $\pi/2$ with respect to each other. Spectra acquired in a single scan at two different fields (f1 and f2) are displayed in Fig. 7b. These fields were chosen such that the peak is at higher and lower frequency, respectively, compared to the reference signal. The quadrature images, the expected positions of which are indicated with arrows, are nearly imperceptible, showing excellent performance of the frequency discrimination. For comparison, the same sample was measured at field f2 with the same NMR frequency offsets and similar acquisition parameters, using a Bruker Avance III console (black traces in Fig. 7c). The spectrum from the low-cost NMR console measured at f2 (i.e. the same spectrum as in Fig. 7b) is shown in gray, over the full range of the spectral window. The signal-to-noise ratio (SNR) of the spectrum acquired by the low-cost NMR console is about 42% of

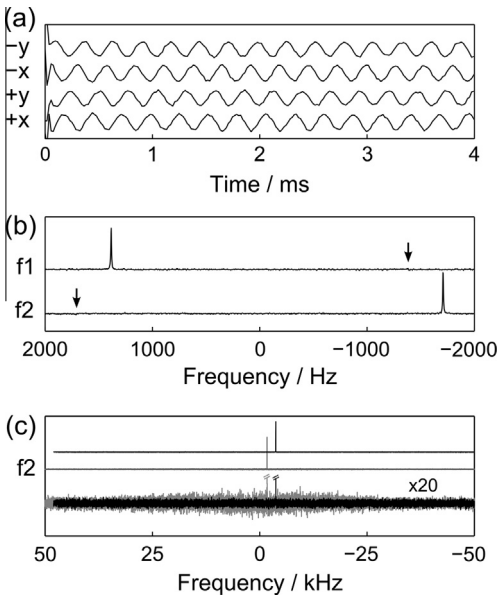

Fig. 7. (a) Phase-shifted FIDs rearranged from a single time-domain data array acquired with 4-step phase cycling on the reference signal, averaging 32 scans (data is shown for a total of 4 ms). (b) f1: The ^{14}N spectrum from a sample of saturated $^{14}NH_4Cl$ with a single scan. f2: The ^{14}N signal of the sample acquired with the magnetic field decreased by 10 Gauss (SNR ~ 74). Spectra are scaled to equal maximum intensity. (c) The f2 spectrum from (b) is shown in gray over the full spectral range. The black trace is a spectrum of the same sample measured using similar acquisition parameters, but with digital quadrature detection, using a Bruker Avance III console (SNR ~ 178). The bottom traces show 20× magnified noise levels.

that of a Bruker Avance III console, despite the fact that NMR signals were sampled at relatively low frequency in the low-cost console. The use of the 50 kHz bandpass filter prior to digitization is responsible for the non-uniform noise level visible in the figure.

The data in Figs. 5–7 are intended as a demonstration of the pulse programming capabilities allowing reproducing typical NMR experiments in the FPGA based NMR console. With accurate control of timing and no restrictions (other than memory length) in the complexity of the pulse program, diverse experiments can be implemented. For instance, two-dimensional homonuclear experiments such as COSY, with coherence selection using phase cycling, are readily feasible. Other experiments of interest may include multi-dimensional spin relaxation measurements, such as T_1–T_2 correlation experiments, or exchange spectroscopy experiments. The former, for example, can be implemented readily by adding an additional π pulse with a variable delay in front of the CPMG pulse sequence to generate a second dimension, and by including appropriate phase cycling [33]. Furthermore, because the pulse sequence execution is achieved by streaming a sequence of machine states to the pulse programming logic, extensions for controlling other hardware are trivial to implement – only the register size for the pulse program events in the FPGA needs to be extended. Thus, it is possible to readily include control for one or more pulsed field gradients by including digital output lines in addition to the one that is already used for switching of the transmitter/receiver circuit. With this addition, various gradient-assisted experiments can be accomplished, such as those for solvent suppression, coherence selection, the measurement of diffusion, or magnetic resonance imaging.

4. Conclusions

In summary, an ultra-low cost approach to an NMR spectrometer is presented. The design is based on a commercial FPGA board, which allows for frequency generation and timing accuracy that is sufficient for medium-to-high frequency NMR. An arbitrary pulse programming capability and the ability to address multiple channels from one board increase its flexibility. Through the use of a common, pre-fabricated board containing the FPGA, the design contains a minimum of external circuit components. We believe that this or similar designs can be implemented inexpensively with the typical knowledge present in many NMR laboratories. Due to the high flexibility in the hardware implementation, they can be tailored to support applications such as relaxometry, polarimetry, diffusometry or NMR based magnetometry.

Acknowledgments

This work was partially supported by a subcontract from the Los Alamos National Laboratory's Laboratory Directed Research and Development (LDRD) program (Project No. 20110166ER).

Appendix A. Supplementary material

Supplementary data associated with this article can be found, in the online version, at http://dx.doi.org/10.1016/j.jmr.2015.02.011.

References

[1] P.S. Belton, A.M. Gil, G.A. Webb, D. Rutledge (Eds.), Magnetic Resonance in Food Science: Latest Developments, Royal Society of Chemistry, 2003.
[2] E. Veliyulin, C. van der Zwaag, W. Burk, U. Erikson, In vivo determination of fat content in Atlantic salmon (Salmo salar) with a mobile NMR spectrometer, J. Sci. Food Agric. 85 (2005) 1299–1304.
[3] H.T. Pedersen, S. Ablett, D.R. Martin, M.J.D. Mallett, S.B. Engelsen, Application of the NMR-MOUSE to food emulsions, J. Magn. Reson. 165 (2003) 49–58.
[4] A. Guthausen, G. Guthausen, A. Kamlowski, H. Todt, W. Burk, D. Schmalbein, Measurement of fat content of food with single-sided NMR, J. Am. Oil Chem. Soc. 81 (2004) 727–731.
[5] R. Lu, X. Zhou, W. Wu, Y. Zhang, Z. Ni, Development of the miniature NMR apparatus for edible oil quality control, Appl. Magn. Reson. 45 (2014) 461–469.
[6] G. Eidmann, R. Savelsberg, P. Blümler, B. Blümich, The NMR MOUSE, a mobile universal surface explorer, J. Magn. Reson. A 122 (1996) 104–109.
[7] A. Legchenko, J.-M. Baltassat, A. Beauce, J. Bernard, Nuclear magnetic resonance as a geophysical tool for hydrogeologists, J. Appl. Geophys. 50 (2002) 21–46.
[8] H. Lee, E. Sun, D. Ham, R. Weissleder, Chip–NMR biosensor for detection and molecular analysis of cells, Nat. Med. 14 (2008) 869–874.
[9] P.T. Callaghan, A. Coy, R. Dykstra, C.D. Eccles, M.E. Halse, M.W. Hunter, O.R. Mercier, J.N. Robinson, New Zealand developments in earth's field NMR, Appl. Magn. Reson. 32 (2007) 63–74.
[10] C. Hilty, S. Bowen, An NMR experiment based on off-the-shelf digital data-acquisition equipment, J. Chem. Educ. 87 (2010) 747–749.
[11] M.F. Isaac-Lam, Analysis of bromination of ethylbenzene using a 45 MHz NMR Spectrometer: an undergraduate organic chemistry laboratory experiment, J. Chem. Educ. 91 (2014) 1264–1266.
[12] G.A. Lorigan, R.E. Minto, W. Zhang, Teaching the fundamentals of pulsed NMR spectroscopy in an undergraduate physical chemistry laboratory, J. Chem. Educ. 78 (2001) 956.
[13] C. Barmet, N.D. Zanche, K.P. Pruessmann, Spatiotemporal magnetic field monitoring for MR, Magn. Reson. Med. 60 (2008) 187–197.
[14] C. Barmet, N. De Zanche, B.J. Wilm, K.P. Pruessmann, A transmit/receive system for magnetic field monitoring of in vivo MRI, Magn. Reson. Med. 62 (2009) 269–276.
[15] B.T. Saam, M.S. Conradi, Low frequency NMR polarimeter for hyperpolarized gases, J. Magn. Reson. 134 (1998) 67–71.
[16] S.R. Parnell, E.B. Woolley, S. Boag, C.D. Frost, Digital pulsed NMR spectrometer for nuclear spin-polarized 3He and other hyperpolarized gases, Meas. Sci. Technol. 19 (2008) 045601.
[17] P. Miéville, S. Jannin, G. Bodenhausen, Relaxometry of insensitive nuclei: optimizing dissolution dynamic nuclear polarization, J. Magn. Reson. 210 (2011) 137–140.
[18] J. Yun, J. Yu, T. Hongyan, L. Gengying, A complete digital radio-frequency source for nuclear magnetic resonance spectroscopy, Rev. Sci. Instrum. 73 (2002) 3329–3331.
[19] S. Handa, T. Domalain, K. Kose, Single-chip pulse programmer for magnetic resonance imaging using a 32-bit microcontroller, Rev. Sci. Instrum. 78 (2007) 084705.
[20] K. Takeda, A highly integrated FPGA-based nuclear magnetic resonance spectrometer, Rev. Sci. Instrum. 78 (2007) 033103.
[21] L. Gengying, J. Yu, Y. Xiaolong, J. Yun, Digital nuclear magnetic resonance spectrometer, Rev. Sci. Instrum. 72 (2001) 4460–4463.
[22] S. Jie, X. Qin, L. Ying, L. Gengying, Home-built magnetic resonance imaging system (0.3 T) with a complete digital spectrometer, Rev. Sci. Instrum. 76 (2005) 105101.
[23] W. Tang, W. Wang, A single-board NMR spectrometer based on a software defined radio architecture, Meas. Sci. Technol. 22 (2011) 015902.
[24] W.K. Peng, L. Chen, J. Han, Development of miniaturized, portable magnetic resonance relaxometry system for point-of-care medical diagnosis, Rev. Sci. Instrum. 83 (2012) 095115.
[25] K. Takeda, OPENCORE NMR: open-source core modules for implementing an integrated FPGA-based NMR spectrometer, J. Magn. Reson. 192 (2008) 218–229.
[26] C.A. Michal, A low-cost spectrometer for NMR measurements in the earth's magnetic field, Meas. Sci. Technol. 21 (2010) 105902.
[27] P. Nath, C.K. Chandrana, D. Dunkerley, J.A. Neal, D. Platts, The "Shim-a-ring" magnet: configurable static magnetic fields using a ring magnet with a concentric ferromagnetic shim, Appl. Phys. Lett. 102 (2013) 202409.
[28] K. Halbach, Design of permanent multipole magnets with oriented rare earth cobalt material, Nucl. Instrum. Methods 169 (1980) 1–10.
[29] G. Bodenhausen, R. Freeman, G.A. Morris, R. Niedermeyer, D.L. Turner, A simple approach to single-channel quadrature detection, J. Magn. Reson. 25 (1977) 559–562.
[30] The GTK+ project, <http://www.gtk.org>.
[31] R. Kaptein, K. Dijkstra, C.E. Tarr, A single-scan Fourier transform method for measuring spin-lattice relaxation times, J. Magn. Reson. 24 (1976) 295–300.
[32] S. Meiboom, D. Gill, Modified spin-echo method for measuring nuclear relaxation times, Rev. Sci. Instrum. 29 (1958) 688–691.
[33] A.E. English, K.P. Whittall, M.L.G. Joy, R.M. Henkelman, Quantitative two-dimensional time correlation relaxometry, Magn. Reson. Med. 22 (1991) 425–434.